FATIGUE BEHAVIOR OF AN ULTRA-HIGH PERFORMANCE CONCRETE I-GIRDER

Justin Ocel, PhD, PSI @ FHWA Turner-Fairbank Highway Research Center, McLean, VA
Benjamin Graybeal, PhD, P.E., FHWA Turner-Fairbank Highway Research Center, McLean, VA

ABSTRACT

Recent advances in concrete materials have led to a new generation of cementitious materials, namely ultra-high performance concrete (UHPC). This concrete possesses advanced properties in terms of compressive behavior, durability, and tensile load carrying capacity. UHPC attains these behaviors via an optimized gradation of cementitious materials, chemical admixtures, and steel fiber reinforcement. Past research conducted by the Federal Highway Administration has characterized the static moment and shear resistance of UHPC superstructure members. The current project aims to investigate the behavior of an AASHTO Type II prestressed girder under repeated cyclic loading. In this test program, the upper limit of the applied cyclic loads is just below the static load levels that would cause flexural and shear cracking of the girder. The specimen endured 12 million cycles without failure and the test was terminated. Cracks were first observed in the cementitious composite after 0.64 million cycles. Additional cracks continued to appear and existing cracks lengthened, but there was no indication that fatigue degradation of the internal fiber reinforcement occurred.

Keywords: Ultra-high Performance Concrete, UHPC, Fatigue, Steel Fiber Reinforcement, AASHTO Type II Girder

INTRODUCTION

The new generation of cementitious materials such as Ultra-High Performance Concrete (UHPC) have enhanced strength properties and internal steel fiber reinforcement which open doors to a new breed of bridge cross-sections. For instance, cross-sections can become much thinner, lighter, and stronger as compared to conventional concrete designs. However, as cross-sectional elements become thinner there is higher likelihood of fatigue susceptibility due to increased primary and secondary stresses in the cross-section.

The research discussed herein is an initial effort to investigate the fatigue behaviors UHPC may exhibit in full-scale prestressed structural members subjected to repeated structural loading. The intention of the study is to investigate the fatigue behavior of both the cementitious composite materials in UHPC as well as the steel fiber reinforcement contained within UHPC. This research is part of a long-term research effort conducted by the Federal Highway Administration (FHWA) to explore the efficacy of introducing UHPC into the US bridge industry.

As part of a previous pilot study, small scale, non-prestressed UHPC samples were subjected to fatigue testing[1]. In this limited study, it was observed that both the cementitious composite as well as the steel fiber reinforcement showed susceptibility to fatigue degradation. Breakage of the steel fiber reinforcement was observed in two precracked prisms cycled at loads from 10 to 60 percent of the cracking load. Flexural cracking of the cementitious composite was observed to occur in one previously uncracked prism after 4 million cycles. These small-scale test showed that, under certain circumstances, fatigue maybe a concern in design.

As an outgrowth of this small scale study and a companion to the structural testing previously completed[2], the full-scale fatigue resistance testing of an AASHTO Type II UHPC girder was initiated. The girder, prestressed with 270-ksi low relaxation prestressing strands, was composed entirely of steel-fiber reinforced UHPC and did not contain any mild steel reinforcement. As such, the testing focused on inducing a large diagonal tensile strain range into the web of the girder. Although flexure fatigue cracks were also likely to occur under this loading configuration, they were considered to be of lesser consequence because the prestressing strands would limit crack opening in addition to providing post-cracking load path redundancy.

EXPERIMENTAL METHOD

The fatigue girder was a standard AASHTO Type II cross-section shown in Fig. 1. The lower bulb contained 24-0.5 inch low-relaxation strands (f_{pu} = 270 ksi) stressed to 0.55 f_{pu}. Twelve of these strands were debonded for the first 36 inches. Two additional strands were placed in the top flange. Since the beam was not manufactured under the control of the researchers, it is not known to what level these two strands were jacked and it was not specified on the design drawing. It was assumed these two strands were not stressed. The UHPC used in the fatigue girder was a Lafarge North America product sold under the trade name Ductal®. The steel fibers were included in the mix design at a concentration of 2 percent by volume. Individual fibers were only 0.5 inches long, 0.008 inches in diameter, and were manufactured to have a minimum ultimate tensile strength of 377 ksi. Further details of the mix design have been published by Graybeal[2].

The load frame is shown in Fig. 2. The specimen was originally part of a 30 foot long girder specimen, half of which was failed in a monotonic shear test. The remaining virgin half of the girder is being tested in this study, with the cantilevered overhang on the west end of the frame being a remnant from the earlier shear test. The section of the specimen used for the fatigue test was unaffected by the prior shear test and no cracks were found prior to cycling. The roller supports were set 168 inches apart and the specimen was loaded in four-point bending using two MTS 220 kip servo valve controlled actuators. Each actuator center was offset 12 inches from the beam's midspan, yielding a 24 inch constant moment region and 72 inch shear spans. In this configuration the beam is subjected to high shear and low moment.

Strain gauges were applied to only one half of the beam. All the gauges were Micro Measurement EA-06-10CBE which has a one inch gauge length. The gauges were primarily focused in three vertical lines centered at 18, 36, and 54 inches from the east support. In each line, there was a longitudinal gauge on the top and bottom extreme fibers, another longitudinal gauge 3 inches down from the top flange, and finally three gauges at the center of the web panel aligned to make a 0/45/90 rosette. Data was collected with an Optim Systems Megadac 3008 acquisition unit, capable of collecting 24 channels of data at very high sampling rates.

FINITE ELEMENT MODELLING

A finite element model was constructed for two reasons; 1) To predict strains from the strain gauges under a static load and 2) To gather an understanding of the true strains in the concrete under the fatigue loads taking into account initial stresses from the prestress strands and self-weight.

Due to symmetry, only half the beam was modeled. Meshing of the model was performed in FEMAP[3] and all analysis and post-processing was performed with ABAQUS[4]. The majority of the model was built with C3D20R elements which are reduced integration, quadratic brick element and very few (0.2% of all elements) C3D15 elements (quadratic, tetrahedron shaped solid) were needed in transition regions. The cantilevered end on the west side was modeled to integrate the proper dead loads into the model. The cantilever was constructed with linear brick elements (ABAQUS C3D8R elements) merged with the quadratic elements using linear multi-point constraints elements. In total, there were 281157 nodes and 69920 elements. The concrete elements were given homogenous, elastic properties with a modulus of 7600 ksi and Poisson's ratio of 0.19, typical properties for UHPC[2]. The prestress strands were taken into consideration, as well as the steel bearing plates under the actuator and atop the support rollers. The modulus of elasticity was assumed to be 28500 ksi for the strand elements and 29000 ksi for the bearing plates, both with a Poisson's ratio of 0.3. The strands were modeled as square cross-sectional elements with side dimensions of 0.391 inches so the strand element had a cross-sectional area of 0.153 square inches.

To predict the strains from the experimental static load, a static analysis was run using the real applied load not considering the prestress force or self-weight. The prestress force and self-weight were neglected because the strain gauges were applied with these stresses already built-in to the beam, hence the strain gauges would not capture those effects.

The model was also used to predict the true strain ranges from the fatigue cycling considering the effect of dead load and the prestress force. The fatigue strain ranges were determined in a three step analysis. The first step was the application of the prestress force. The model did not consider the sequential construction of the beam, rather the concrete elements and steel prestress elements were generated together and initial stress were applied to only the prestress strands. When applying initial stresses in ABAQUS an analysis step is required for the model to equilibrate itself due to any unbalance from the applied initial stresses. The strands in the real beam were only jacked to 55% of f_{pu}. After accounting for prestress losses it was assumed the final stress in the strands was 125 ksi. To attain a final strand stress of 125 ksi an initial stress of 135 ksi needed to be applied to the strand elements. Essentially, the 10 ksi difference accounts for the elastic shortening of the beam. The second step was the application of the lower fatigue load and the final step was the application of the upper fatigue load.

STATIC TESTING

Prior to fatigue cycling, at static test was run on the beam to ensure the loads were being distributed as expected. The static loading used a simple ramp loading of each actuator from 10 to 100 kips and back to 10 kips. This ramp was run five times and the strains at the peak load were averaged to cancel out hysteretic effects in the strain gauges. Shown in Fig. 3 is a pictorial representation of the data produced by the strain rosettes placed in the center of the web panel along three different lines in the shear span. The figure shows the principal strains on a rotated element calculated from the three gauges of each rosette. Also shown are the results from the static finite element model analysis. The strains collected from the gauges follow closely the predictions of the finite element model. Shown in Fig. 4 are the strain profile plots through the depth of the beam along each gauge line. Also shown are the same strain profiles extracted from the finite element model. Each of the two figures show close agreement between the strain gauges and the finite element indicating the loads are being distributed as expected and that the finite element model was sufficiently refined to predict strain.

FATIGUE CYCLING

Cycling began in September 2006 with each actuator cycling between 30 and 200 kips. The upper load level was chosen to be 200 kips as it both created a principal tensile strain in the web that was less than but close to the cracking strain and was within the capacity of the available testing equipment. The lower load was chosen to create a state of zero principal strain in the web. The upper load is also just below that needed to form flexure cracks based on previous monotonic testing on an identical cross-section. In total, this load range creates a large stress (or strain) range in the web without stress (or strain) reversal.

The actuators were cycled between 0.75 and 1.25 Hz. The loading rate fluctuated early in the cycling to find an optimum cycling rate. The majority of the cycling was completed at 0.75 Hz.

Locating cracks in UHPC is significantly more difficult than would be expected for conventional concretes. Crack widths may be as small as 0.0005 inches. The primary method used in this research project to locate cracks on the surface of the girder was to spray a volatile liquid on the surface and allow evaporation of the liquid to provide a temporary indication of any crack location. Denatured alcohol was the preferred volatile due to its moderate rate of evaporation and its lack of objectionable odor. Once the first cracks were identified, inspections were performed every 0.1-0.25 million cycles. Only the south facing side of the girder was inspected for cracks because instrumentation installed on the north face made the inspection too difficult. During each inspection, the denatured alcohol was sprayed on the surface and any crack extensions were identified with pencil. After the beam had endured 3 million cycles, the inspection interval was increased to every 1 million cycles due to a decreased rate of new crack formation.

In a few locations the crack widths were monitored. When the cracks first formed some the widths ranged from 0.0005 to 0.001 inches. The width was measured with a hand-held crack width microscope, however it only had 0.001 inch graduations by which to make measurements against. Even though some monitored cracks did extend throughout the cycling, these cracks were not observed to grow measurably wider.

The first observable cracks were noted at 0.640 million cycles. The cracks formed (shown in Fig. 5) in the east shear spans at the radius transition between the web panel and the lower bulb. After 1.405 million cycles, the same type of cracks at the transition between the web and lower bulb formed in the west shear span (shown in Fig. 6). The first flexure cracks were noticed in the constant moment region after 1.888 million cycles (shown in Fig. 7). When the flexure cracks were noticed, so was a very long longitudinal crack in the bottom flange, extending the length of the constant moment region. The investigation of the bottom face of the girder revealed longitudinal cracks running along the length of the beam correlating to the location of the prestress strands.

Figures 8 through 11 show the continued growth of the cracks through 12 million cycles. The existing cracks continued to grow in this time period, primarily creating compression struts from the supports to the load points. In addition, further cracks formed in the transition between the web panel and upper flange bulb.

ANALYSIS OF FATIGUE CRACKING

Cracks were anticipated to form in the web panel based on high shear stress range applied to the beam. However, cracks did not form symmetrically on the east and west spans nor did the first cracks initiate in the web panel. Instead, the first cracks formed in the east shear span and at the intersection between the bottom flange bulb and web panel. Two reasons exist that can explain this cracking. First, the cross-section is irregularly shaped with many stress risers, such as the fillet transition from the lower bulb to the web panel. Second, the fatigue girder was the end section of a much longer girder and the east shear span was the end of the original girder. During the construction of the girder, 12 of the 24 strands in the lower bulb were debonded for 36 inches to reduce the stress concentration at the end of the girder. Thus, there was a reduced precompression in part of the east shear span.

Shown in Fig. 12 is a schematic of the beam with the cracks after 0.640 million cycles superimposed with a maximum principal strain contour map from ABAQUS. The contour map only plots positive (tensile) principal strains from the model with the prestress, dead load, and 200 kip actuator forces applied. These are shown because cracks in concrete form in areas of high principal tensile strain and would therefore be an indicator of where cracks would first form under this loading configuration. The highest strain contours appear on the east and west sides of the beam at the transition between the web panel and lower flange bulb. The contour plot also shows the effect of the debonded strands on the east side as the area of the peak strain contour is larger on the east side.

Also shown in Fig. 12 are fictitious rotated elements showing the principal strains and orientations at two points on the east and west sides of the beam where they are a maximum. The principal strains are shown for the two cases with 30 and 200 kips of force from each actuator (i.e. the minimum and maximum fatigue loads applied to the beam). These elements show that as the beam is fatigued the principal strains change direction by 18 to 25 degrees during a full cycle of load. This is because with only 30 kips of actuator load the girder is dominated by flexural behavior (after accounting for prestress force and dead load) and dominated by shear at the upper 200 kip fatigue load. The state of strain at the upper and lower fatigue loads can then be used to determine a tensile strain range in the vicinity of the cracks. The orientation of the principal tensile strain at the upper fatigue load was used to calculate the tensile strain range between the upper and lower fatigue loads. This leads to a tensile strain range that caused first cracking of 201 $\mu\varepsilon$ on the east side of the beam and 181 $\mu\varepsilon$ on the west side.

In addition to the shear cracks, flexure cracks also formed. Since the flexure cracks initiated at the extreme bending fiber and grew upwards into the beam, the principal strains at the extreme bending fiber need to be considered. Figure 13 shows a plot of the total longitudinal strains (with prestress, dead load, and actuator forces) on the extreme tension fiber as a function of distance from the center of the east roller support. Each plot (for 30 and 200 kip actuator forces) has two distinct peaks which arise because the debonded strands on the east side of the beam engage and add additional compressive force to the cross-section. Note that for this analysis the strand elements were fully coupled to the concrete elements so that it took approximately 8 inches to fully transfer their prestress force into the concrete. This plot shows that the strains in the flange are strictly compressive with only 30 kips of load from each actuator. In most circumstances, fatigue cracks propagate under tensile strain and it is quite common to neglect the portion of the strain cycle in compression. Even with the 200 kips of force from each actuator the only portion of the lower flange that has tensile strains is in the center third of the span. Therefore, the maximum strain range in the flange is 172 $\mu\varepsilon$ when only accounting for the tensile portion of the strain range.

Fatigue cracks initially formed in three locations at different cycle counts; shear cracks at the transition between web panel and lower flange on the east and west shear spans and flexural cracks in the constant moment region. There is no well defined procedure to assess the fatigue resistance of a steel fiber reinforced cementitious materials of this type. The AASHTO S-N approach has served the steel bridge industry well for over 25 years. In this approach, fatigue is only dependant upon stress range (S) at a detail and the number of cycles to failure (N) hence the “S-N” approach. When experimental data is plotted in terms of the stress range versus the number of cycles it tends to follow negative exponent power laws. These curves are commonly presented in logarithmic space where they plot as straight lines. These curves have been defined for welded steel details but they have also been extended to evaluate bolted connections and prestress strand. As a first attempt to define the fatigue resistance of UHPC, a modified version of the S-N approach will be used. Since concrete is a brittle material it fails via principal tension, hence why in the previous paragraphs the tensile strain range was evaluated at the three locations fatigue cracks first formed. These strain ranges and cycles counts were plotted in logarithmic space in Fig. 14. The technique of plotting strain ranges and cycle count has been used by the offshore industry when defining the fatigue resistance of tube-to-tube connections with hot-spot strain readings from strain gauges[5]. For simplicity, linear constitutive material models are then used to convert strain ranges into stress ranges (i.e. strain ranges are multiplied by the modulus of elasticity to attain stress ranges). This same technique was used in Fig. 14 where the stress range axis was defined by multiplying the strain range scale by 7600 ksi (i.e. the typical modulus value for UHPC). Also shown in this plot are the AASHTO S-N curves for steel which are based on the stress range scale. Again, the AASHTO S-N curves defined for welded steel details are presented for reference only and should not be used to classify UHPC materials. The UHPC experimental points plot much lower than Category E’ curve, thus presenting the apparent conclusion that UHPC has poor fatigue resistance. However, it would be more reasonable to consider these data points in terms of the tensile cracking stresses normally associated with cementitious materials. Interestingly, the three UHPC experimental points do follow a linear relationship in log space, but this observation is only defined by three points and therefore no firm conclusions can be made as fatigue data typically exhibit significant scatter.

CONCLUSIONS

This research was conducted to evaluate the fatigue resistance of a prestressed UHPC girder. Since the beam was made of UHPC it allowed for a design with no mild steel stirrups to assist with shear resistance. Previous research on a limited number of non-prestressed, small scale UHPC specimens demonstrated that fatigue degradation of both the UHPC cementitious composite as well as the steel fiber reinforcement was possible. This research was intended to investigate whether fatigue degradation is a viable concern for UHPC I-girders containing no mild steel reinforcement in their web panel. The girder was subjected to very large shear load ranges in order to develop these types of shear fatigue cracks. The beam endured 12 million cycles with a 170 kip shear load range and had yet to reach a catastrophic failure. Multiple cracks developed during the application of these cycles, but there was no noticeable change in the global behavior of the girder, no auditory- or surface strain-based indication of fatigue damage to the prestressing strands, and no auditory- or crack width-based indication of fatigue damage to the fiber reinforcement bridging the cracks in the cementitious matrix.

FUTURE WORK

The AASHTO Type II girder tested in this research program demonstrated unusual crack patterns, likely because of stress risers in the cross-section and non-uniform prestress force from debonded strands. Given that this test program has demonstrated that the UHPC cementitious matrix may be susceptible to fatigue degradation (or at least reduced tensile strength under repeated loading), a larger UHPC fatigue testing program has been developed. The program will be executed from summer 2007 through fall 2008. Six inch wide and 15 inch tall rectangular prestressed beams will be fabricated and tested under cyclic four-point bending loads. The specimens will be subjected to different load ratios to establish a fundamental base of fatigue resistance of the UHPC material.

REFERENCES

1. Graybeal, B. A., Hartmann, J. L., "Ultra-High Performance Concrete Material Properties," Proceedings of the 82nd Annual Meeting of the TRB, Washington DC, January 2003.
2. Graybeal, B. A.; "Structural Behavior of Ultra-High Performance Concrete Prestressed I-Girders," Report No. FHWA-HRT-06-115, Office of Infrastructure Research and Development, McLean, VA, August 2006.
3. FEMAP, FEMAP User Guide, ver. 9.0, (Plano, TX: UGS Corporation, 2005).
4. ABAQUS, ABAQUS ver. 6.5, (Providence, RI: ABAQUS Inc., 2004).
5. Marshall, P. W., "*Design of Welded Tubular Connections, Basis and Use of AWS Code Provisions*," Elsevier Science Publishers, 1992.

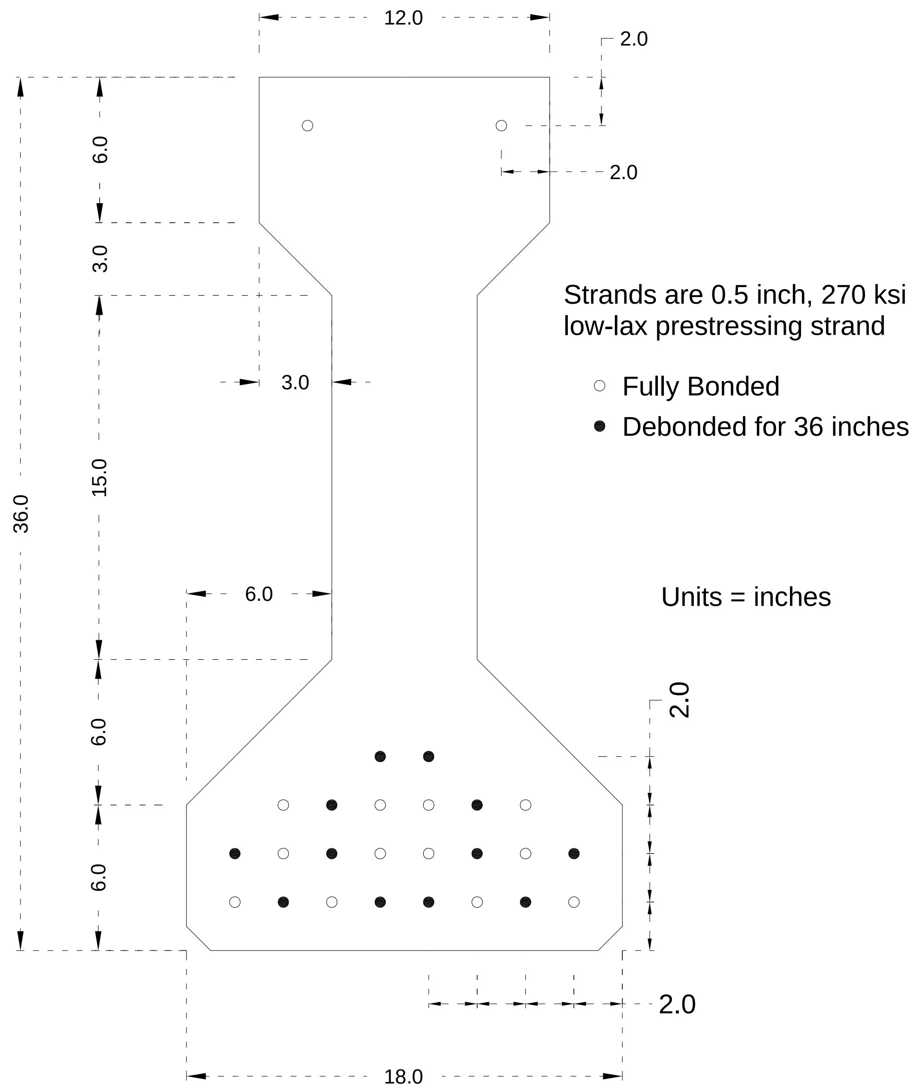

Fig. 1. AASHTO Type II cross-section.

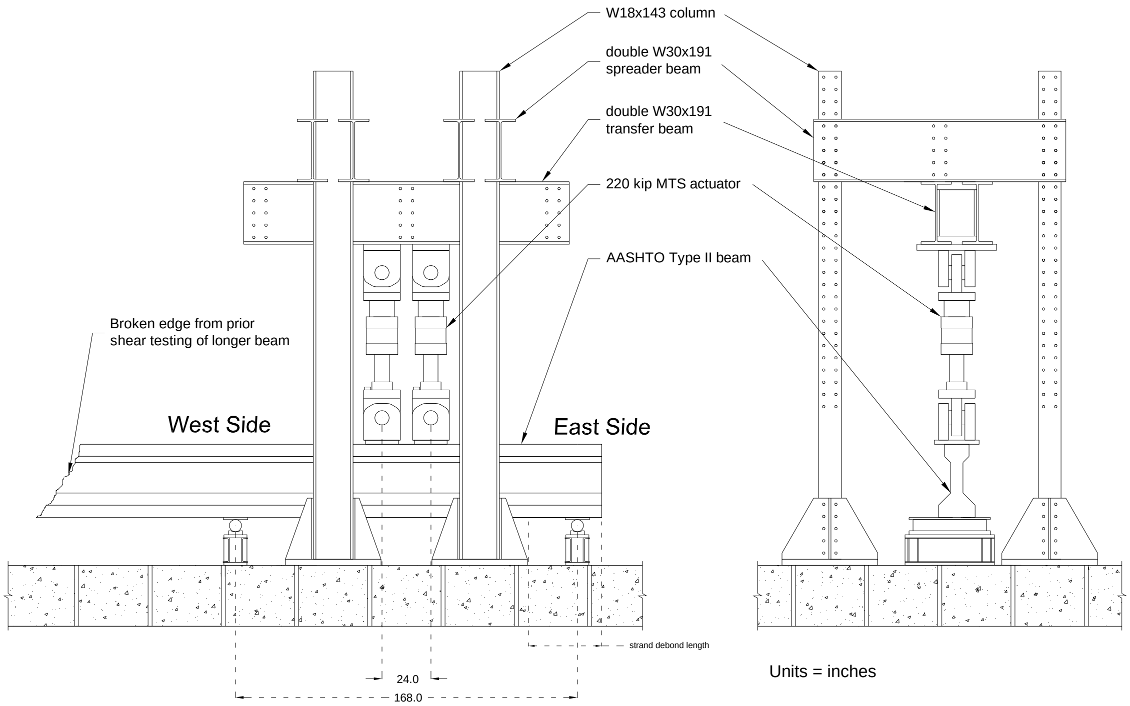

Fig. 2. Fatigue load frame.

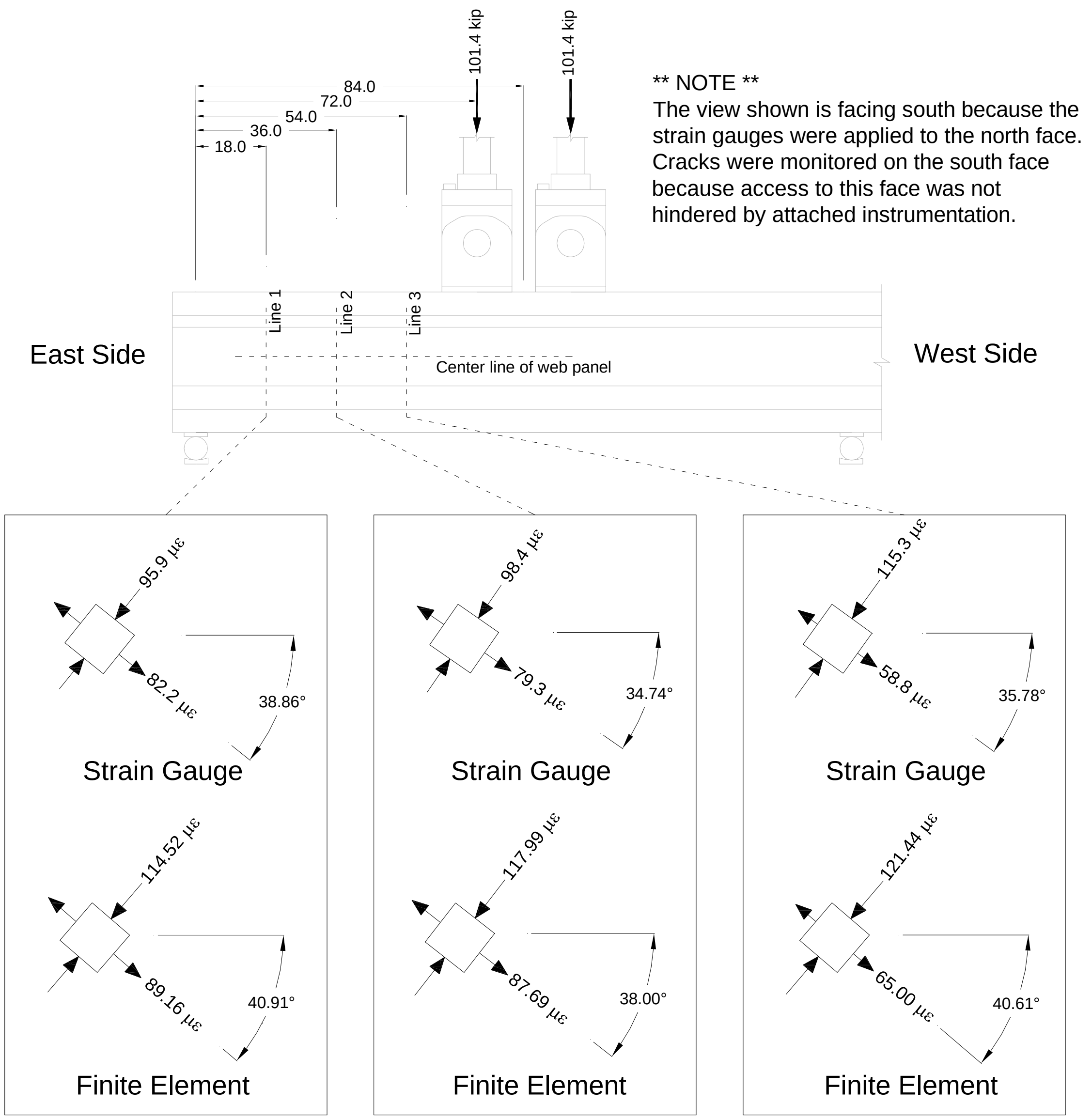

Fig. 3. Results from strain rosettes at center of web panel.

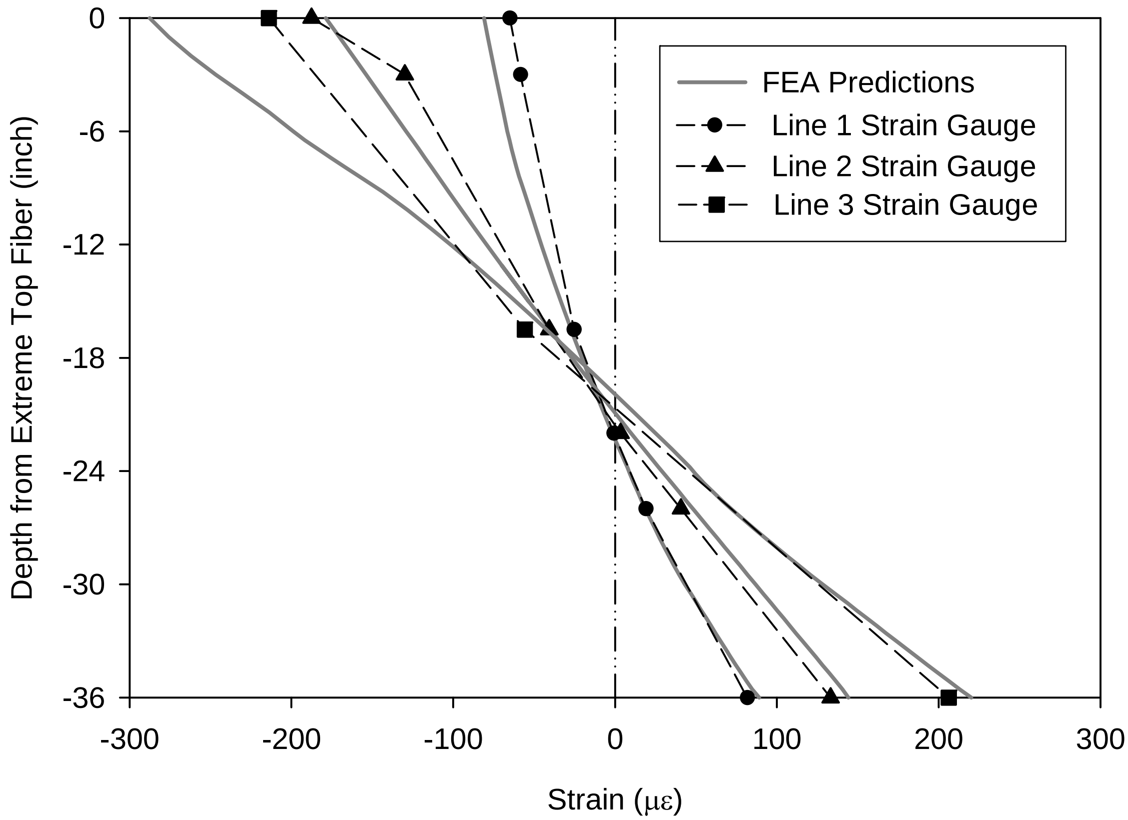

Fig. 4. Strain profiles through beam depth at three lines in shear span.

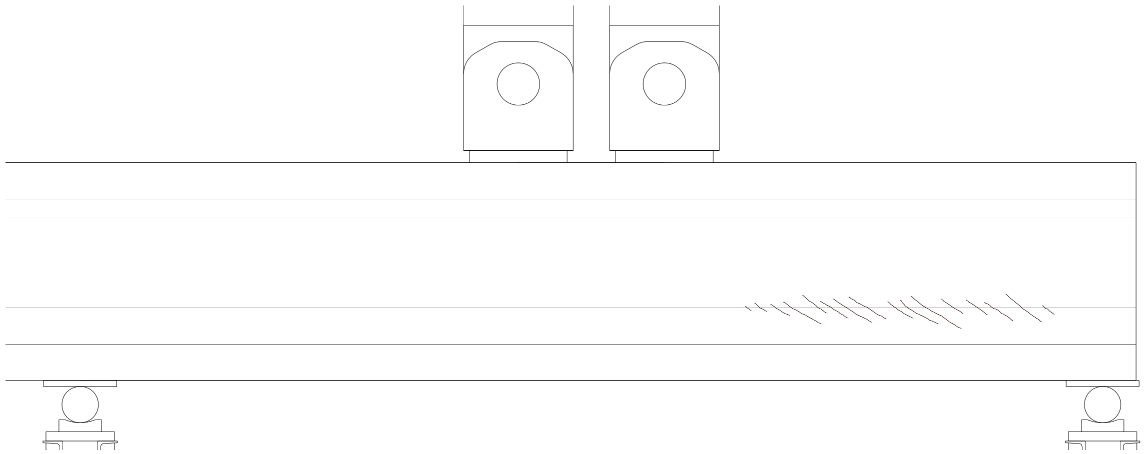

Fig. 5. Crack pattern observed after 640,000 cycles.

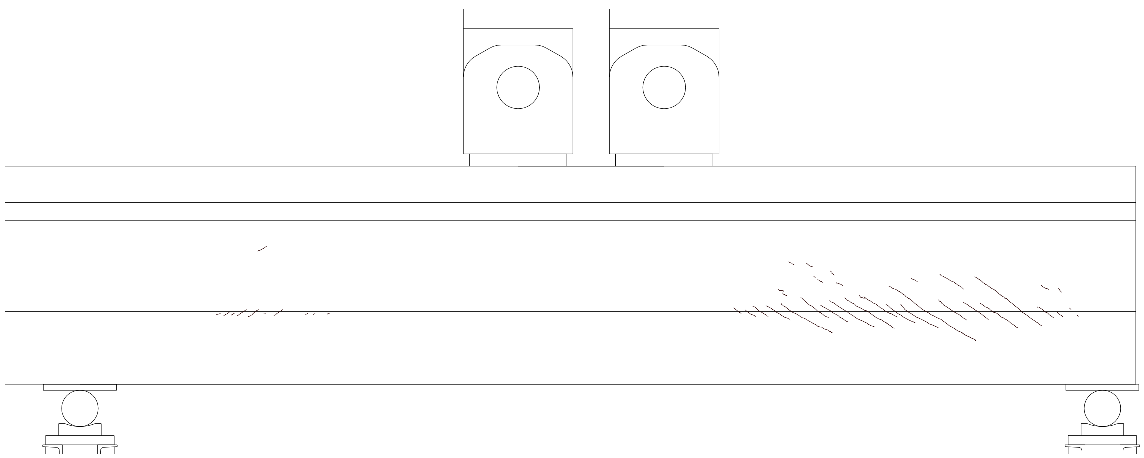

Fig. 6. Crack pattern observed after 1.535 million cycles.

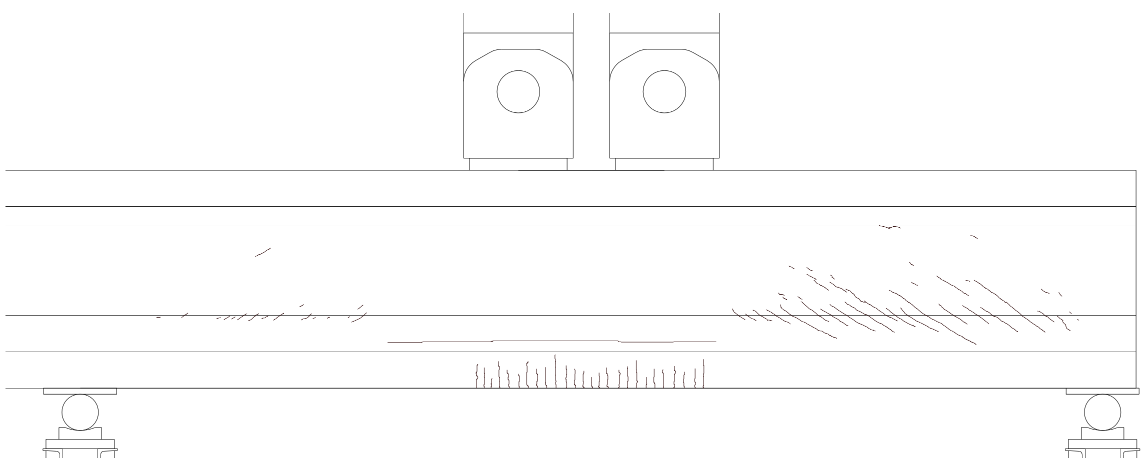

Fig. 7. Crack pattern observed after 2.145 million cycles.

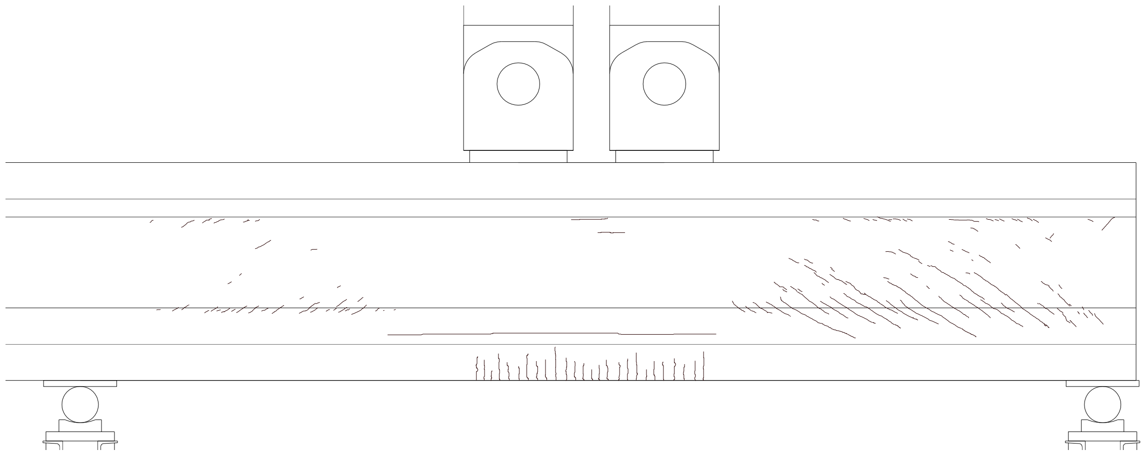

Fig. 8. Crack pattern observed after 4.087 million cycles.

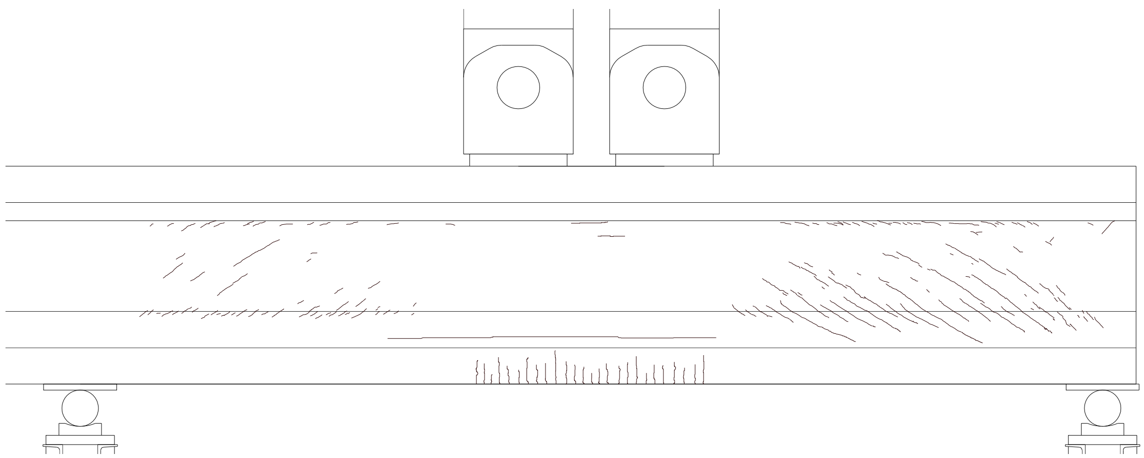

Fig. 9. Crack pattern observed after 5.946 million cycles.

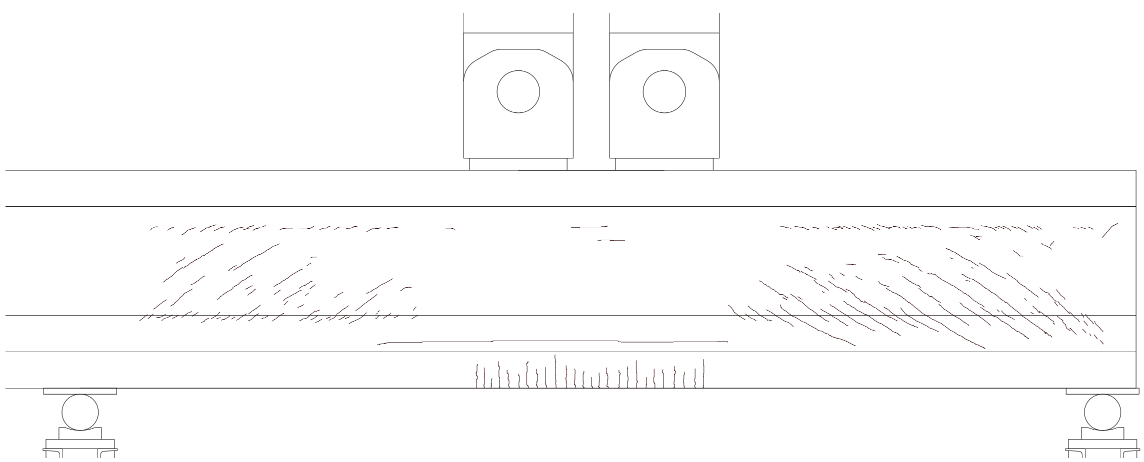

Fig. 10. Crack pattern observed after 8.107 million cycles.

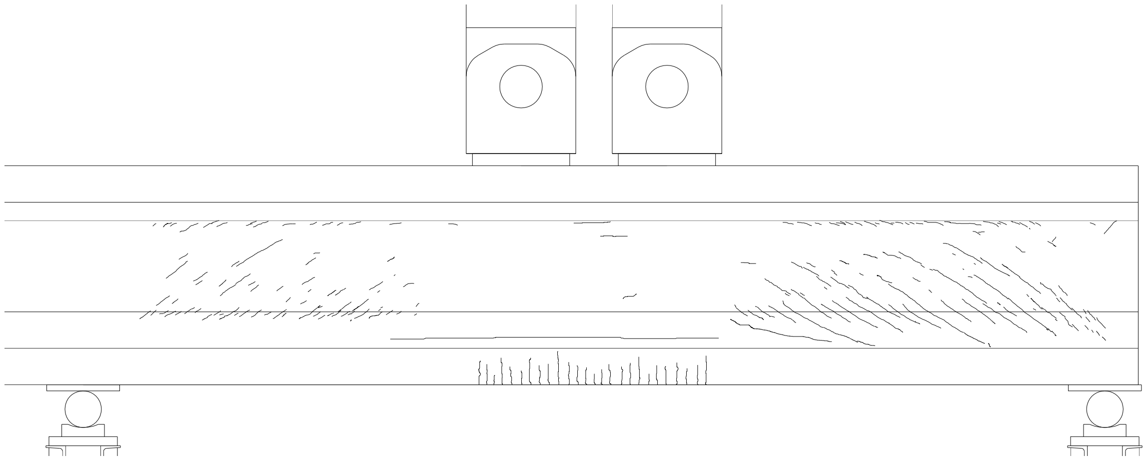

Fig. 11. Crack pattern observed after 11.993 million cycles

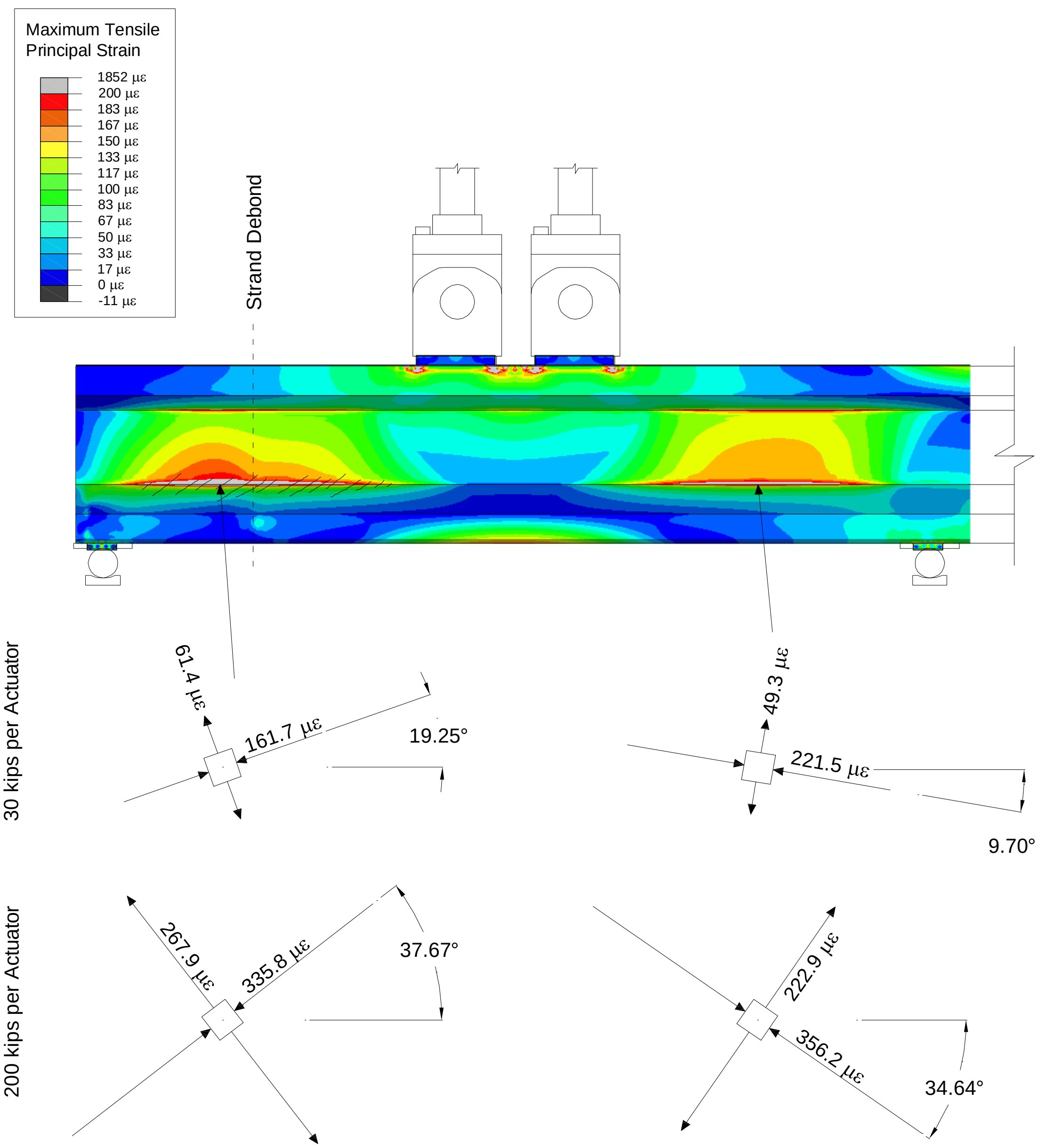

Fig. 12. Maximum principal strain contours shown with maximum strain on a rotated element.

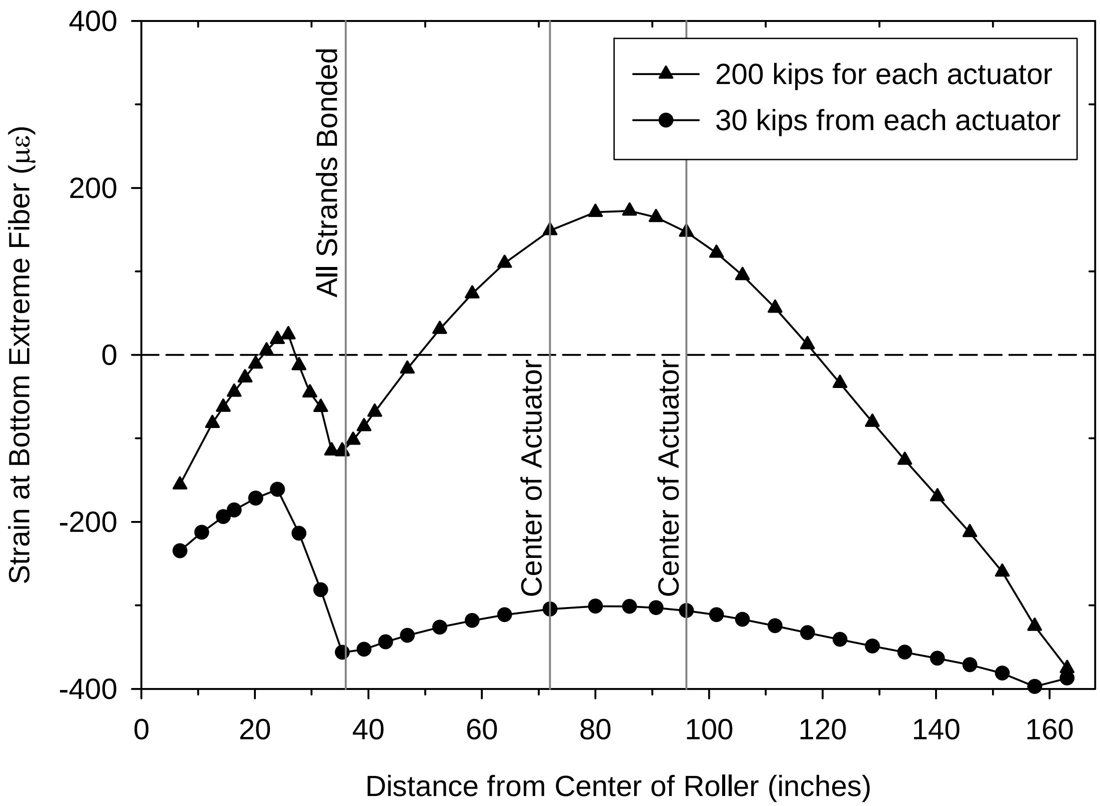

Fig. 13. Total longitudinal strain distribution along extreme tension fiber (bottom flange) under minimum and maximum fatigue loads.

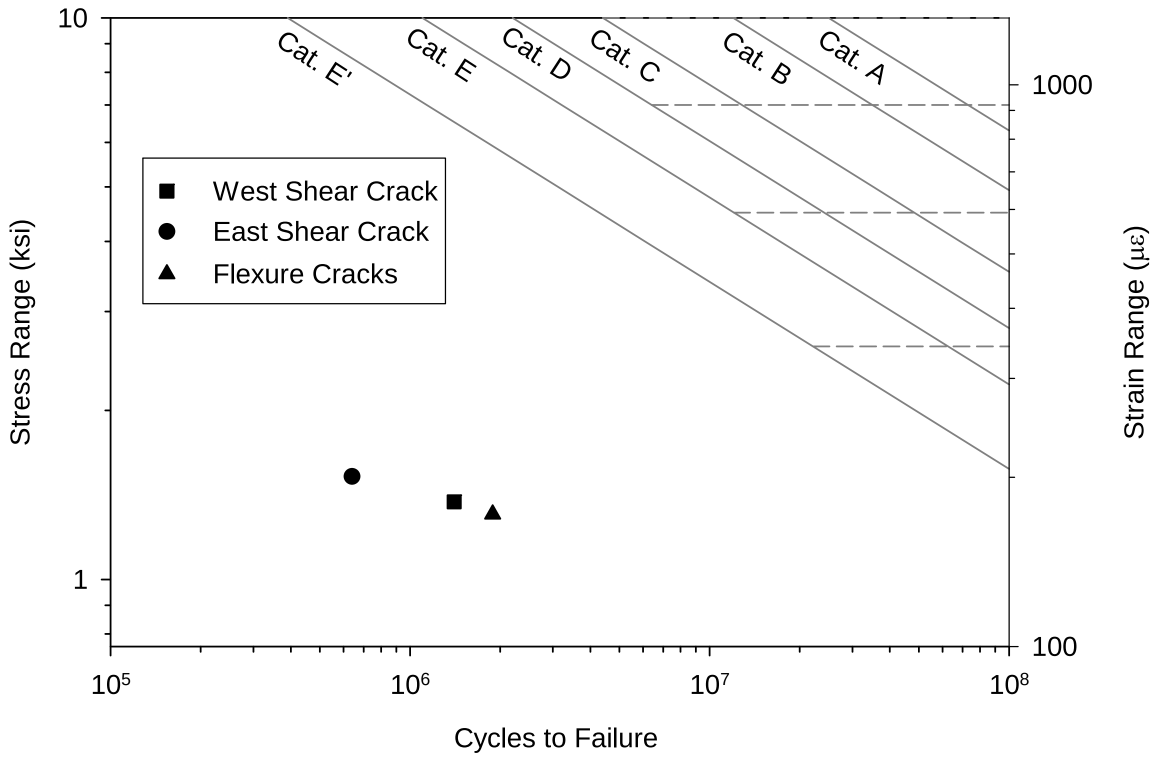

Fig. 14. AASHTO S-N plot of three initial fatigue cracks in UHPC girder.